Supplemental Materials

Molecular Biology of the Cell

Nguyen et al.

Supplemental Information

Supplemental Movie

Movie S1: 3D coarse-grained simulations of the contractile actomyosin ring. This movie shows (i) the elements and properties of our 3D coarse-grained model of the contractile ring, (ii) building the initial model, (iii) exploration of different actomyosin configurations, and (iv) final model that best agreed with experimental data.

Movie link: http://lab.jensengroup.org/lam/sim/MovieS1.mp4

Supplemental Figures

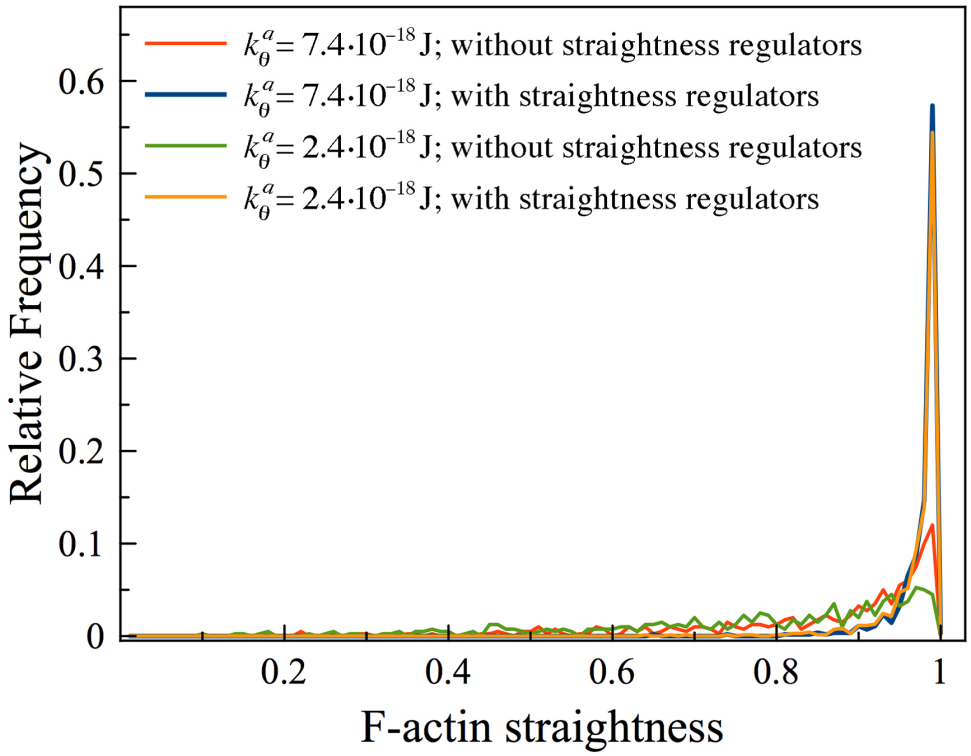

Figure S1: Histograms of straightness factors for simulated filaments show that straightness regulators were required to prevent filament bending, and the same result obtained even when the actin bending stiffness k_θ^a was reduced three-fold.

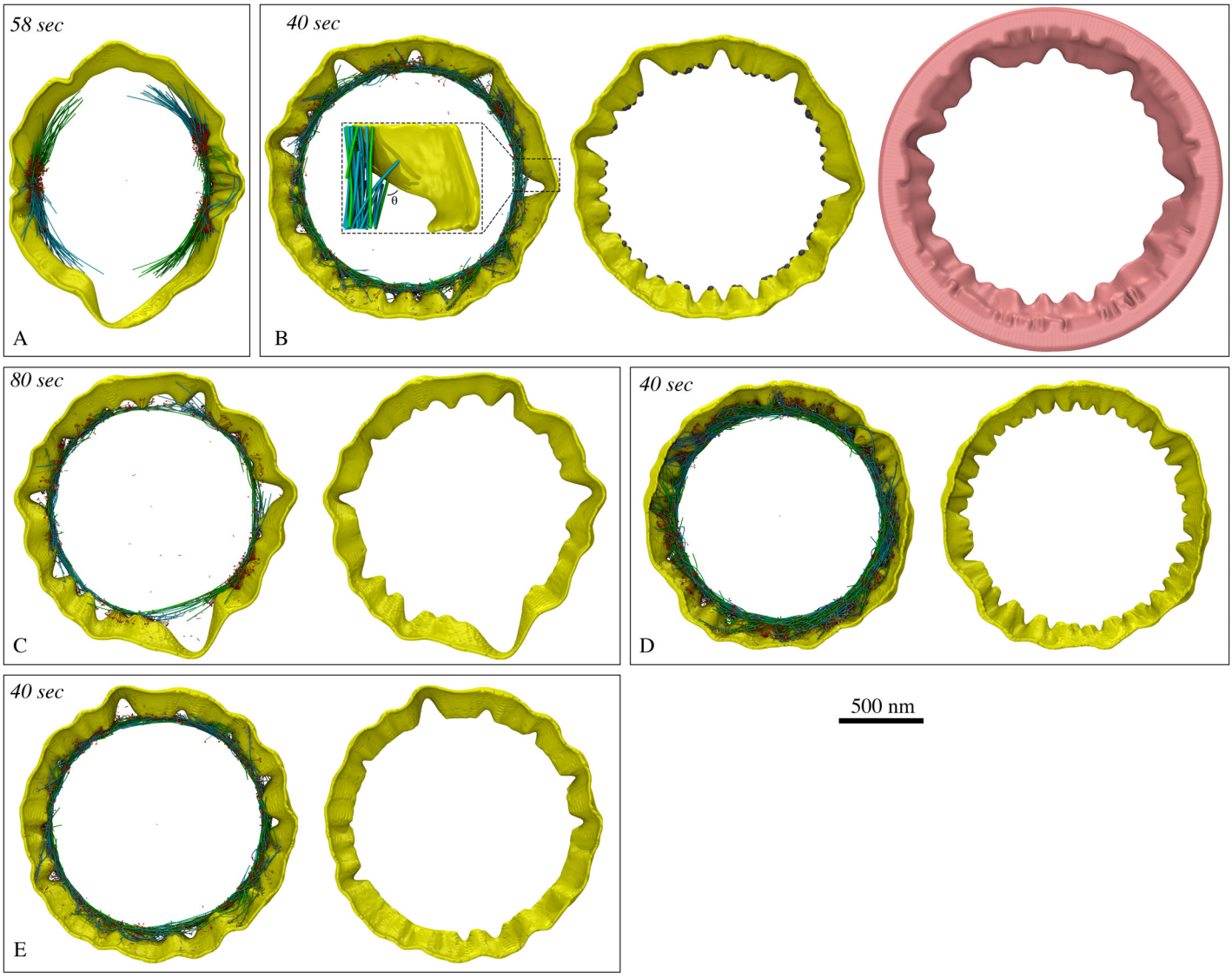

Figure S2: Extended simulation results of model 1 with different parameters. (A) Without crosslinkers, nodes could constrict the membrane, but the ring was broken eventually. (B) Addition of crosslinkers maintained the ring integrity (left), but concentration of the constriction force on a limited number of nodes caused a puckering defect of the membrane (middle) and the leading edge of the septum (right). Zoomed-in view in the left panel shows how, as a consequence, F-actin makes a large angle with respect to the membrane. Puckers also formed when the concentrations of actin, myosin, and crosslinkers were reduced in half (C) or doubled (D), or the number of nodes increased from 64 to 140 (E).

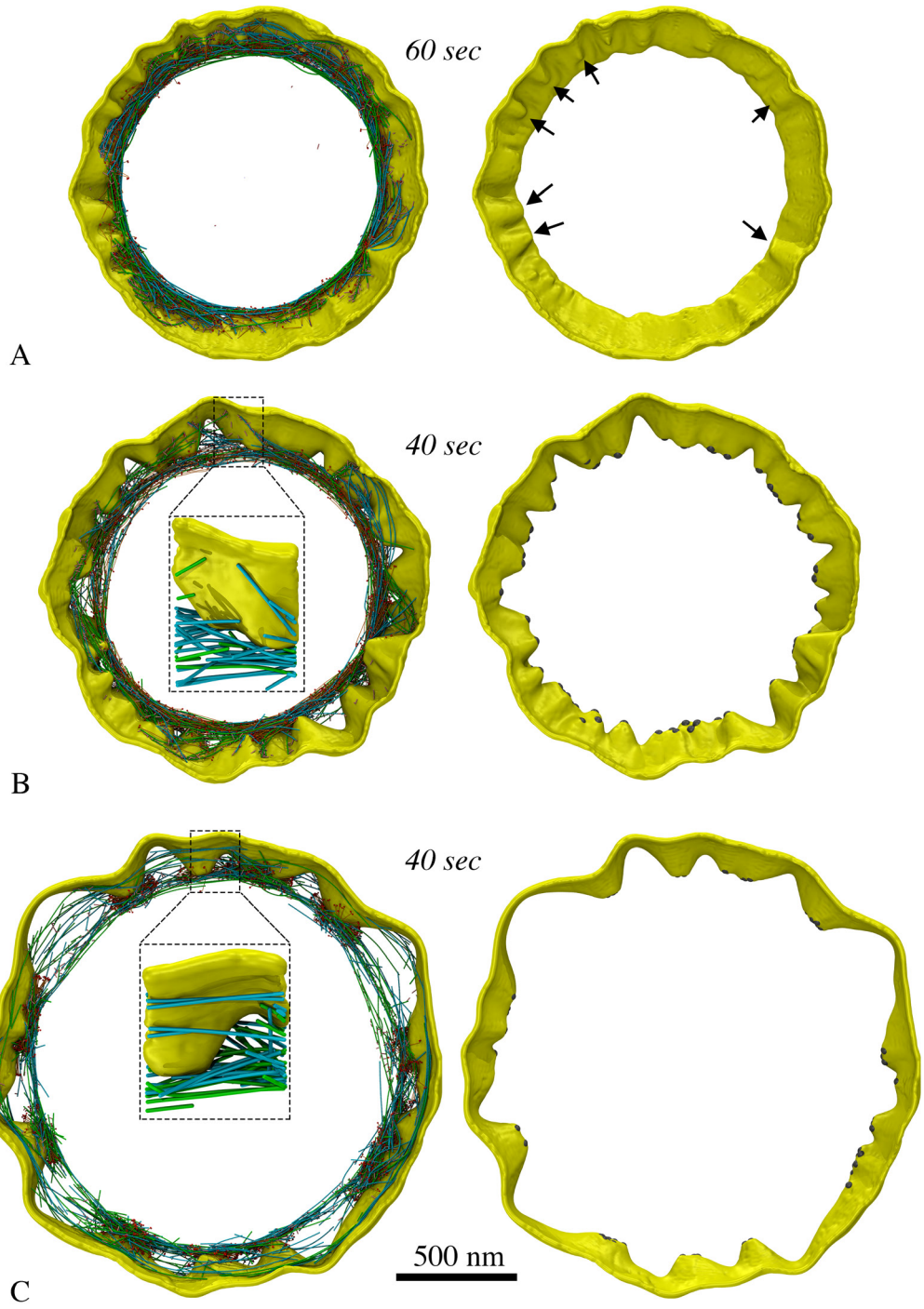

Figure S3: Enlarged views and additional views of membrane defects due to the presence of nodes. (A) Simulation result of model 2. Breaking the nodes of unipolar myosin into pairs mitigated the membrane defect, although small puckers were still observed (arrows). Simulation results of (B) model 4 and (C) model 13 show that tethering the ring to the membrane via a limited number of nodes again caused membrane puckering, and as a consequence, F-actin was often seen making a large angle with respect to the membrane (zoomed-in view).

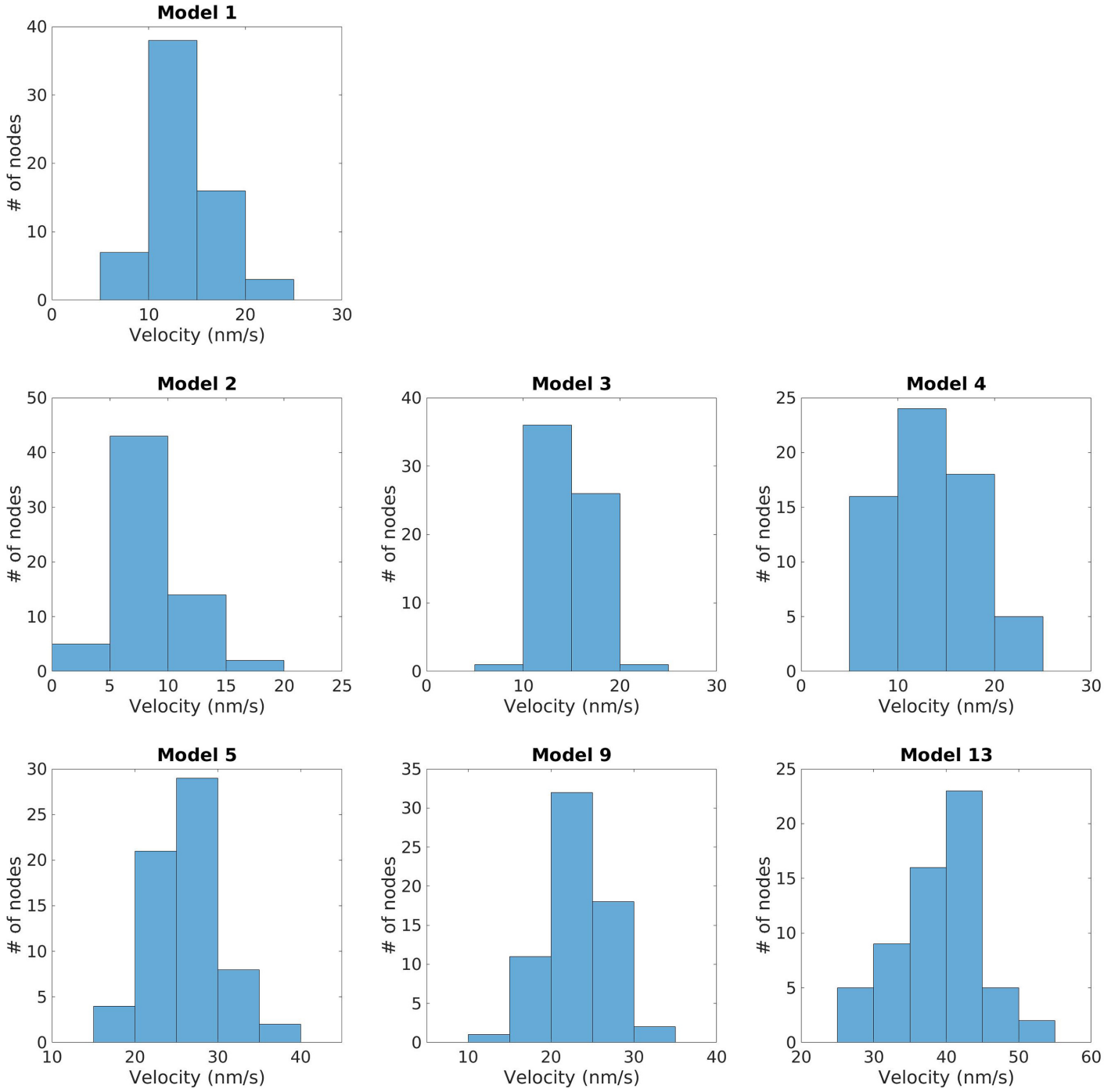

Figure S4: Histograms of node circumferentially-sliding velocity of: (top) model 1, where both actin and unipolar myosins were attached to membrane-bound nodes, (middle) models 2, 3, and 4, where only actin filaments were attached to nodes, and (bottom) model 5, 9, and 13, where only unipolar myosins were attached to nodes.

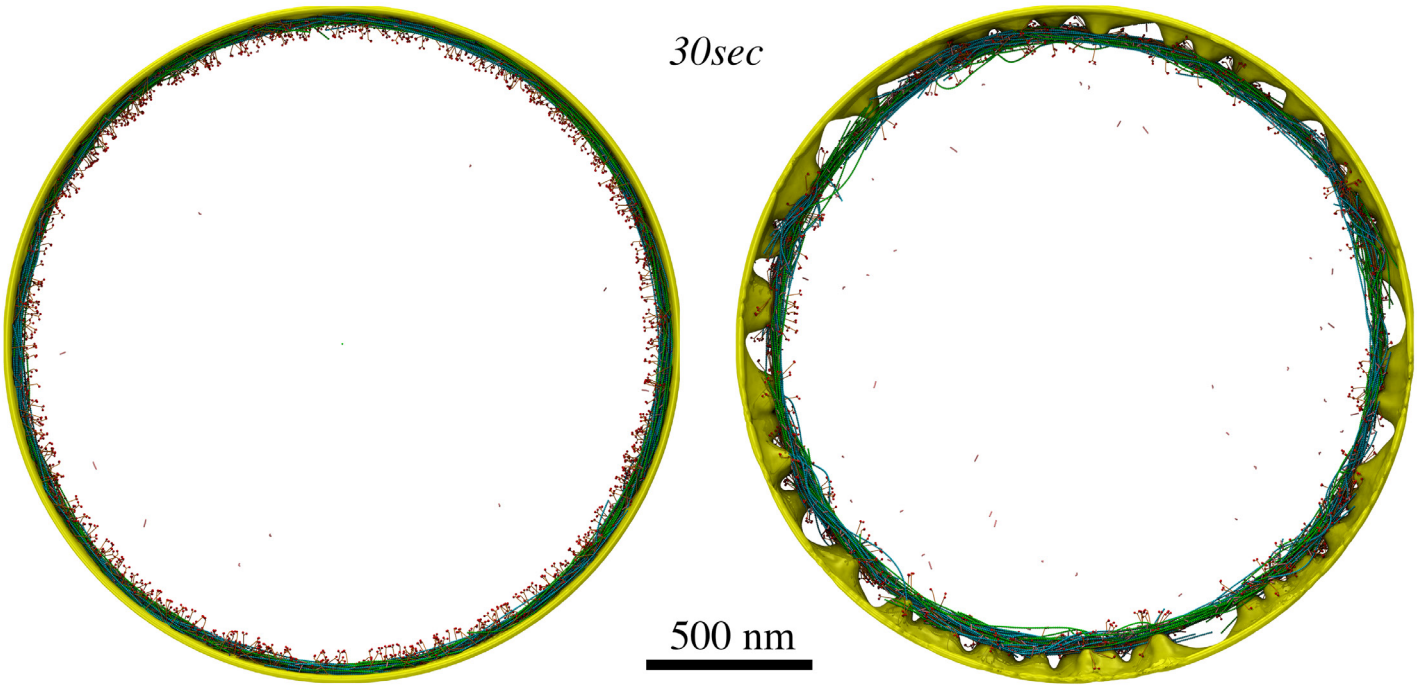

Figure S5: Effect of reducing the mechanosensitivity on cell wall growth. As the minimal radial force on a membrane bead that induces cell wall growth was increased 100 times, cell wall growth was completely suppressed in model 7 where unipolar myosins were individually connected to the membrane (left), but membrane puckering still occurred in model 1 where actin filaments and unipolar myosins were connected to the membrane-bound nodes (right).

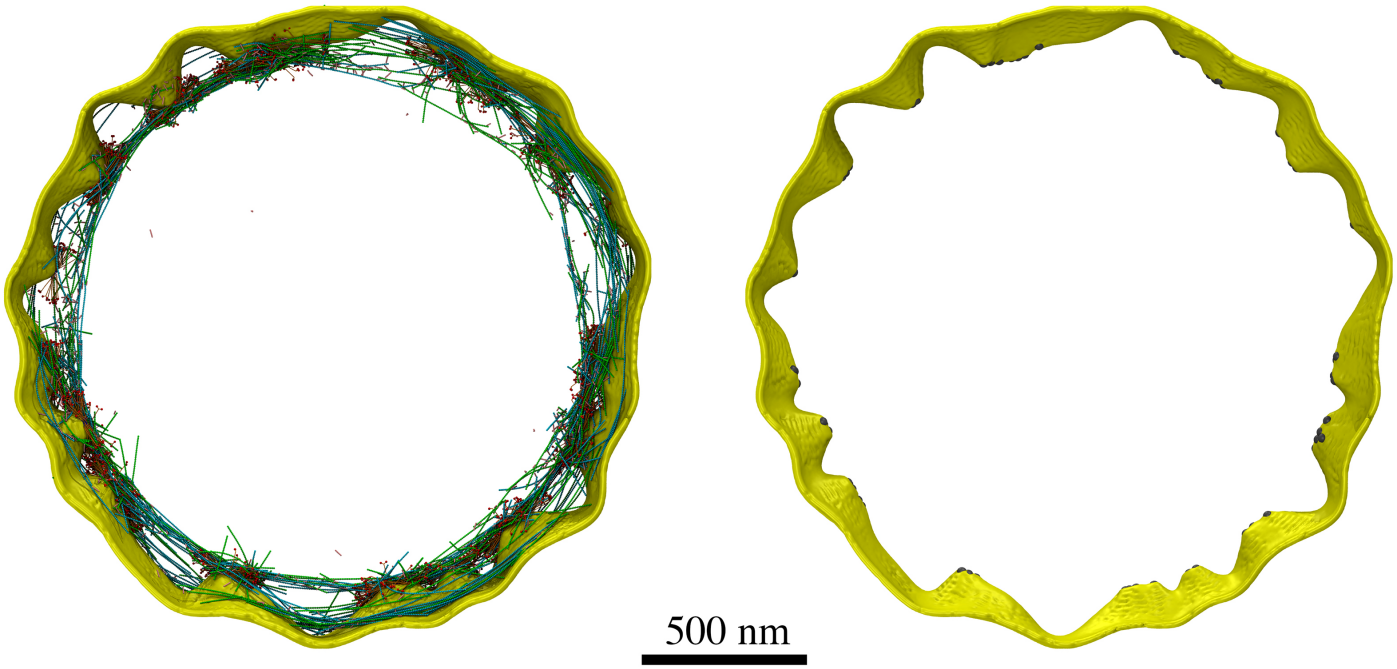

Figure S6: Simulation results of model 13 (actin was not connected to the membrane and unipolar myosins were at nodes) without the rule that myosin could bind to actin only if the filament was crosslinked upstream. Puckers were obvious after 40 sec of the simulated time.

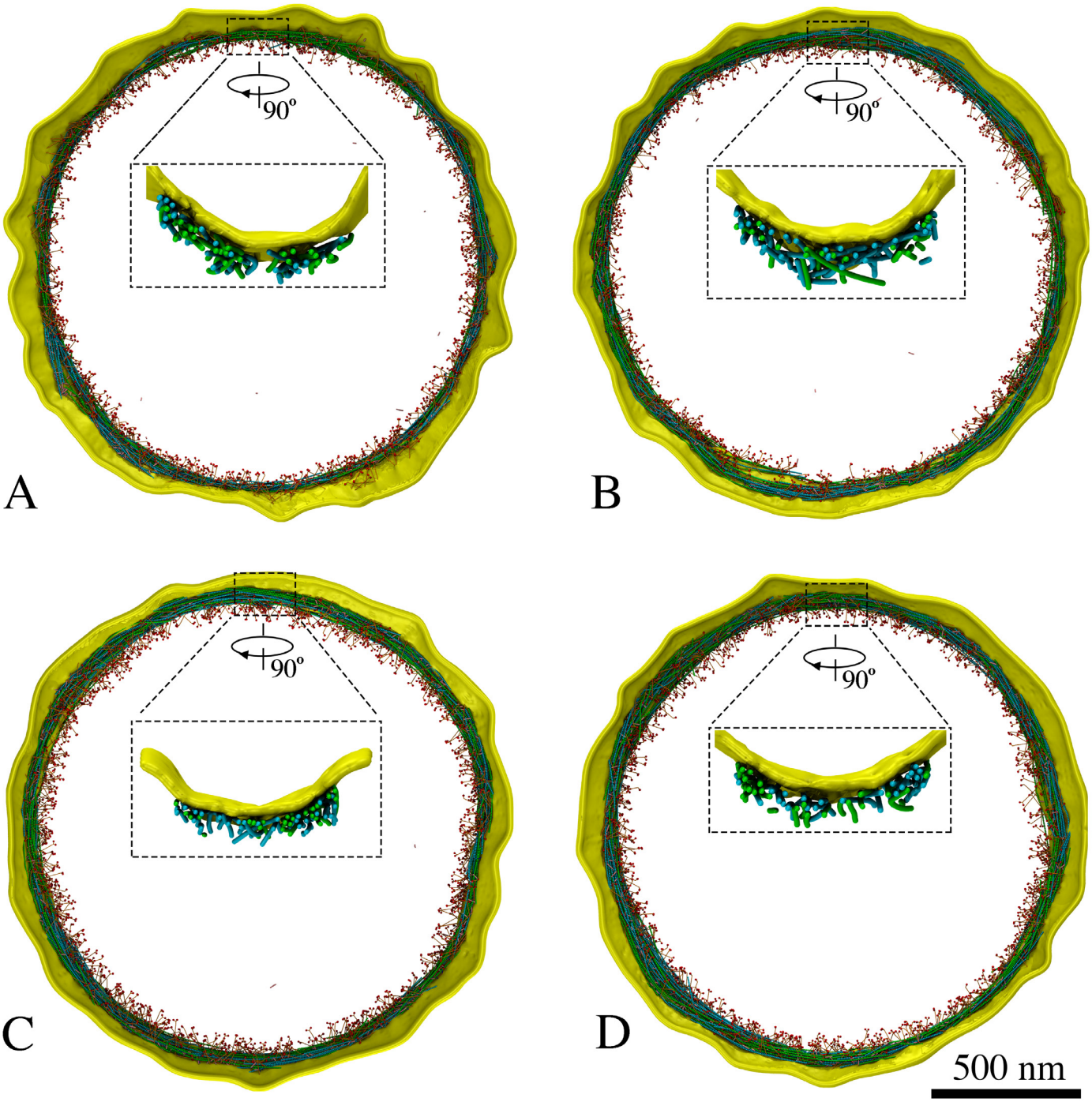

Figure S7: Enlarged views and additional views of model 3 (A), model 7 (B), model 11 (C), and model 15 (D) after 80 sec of the simulated time. The homogeneous distribution of individual membrane-attached unipolar myosins helps maintain membrane smoothness and circularity, but F-actin was kept close to the membrane (zoomed-in views).

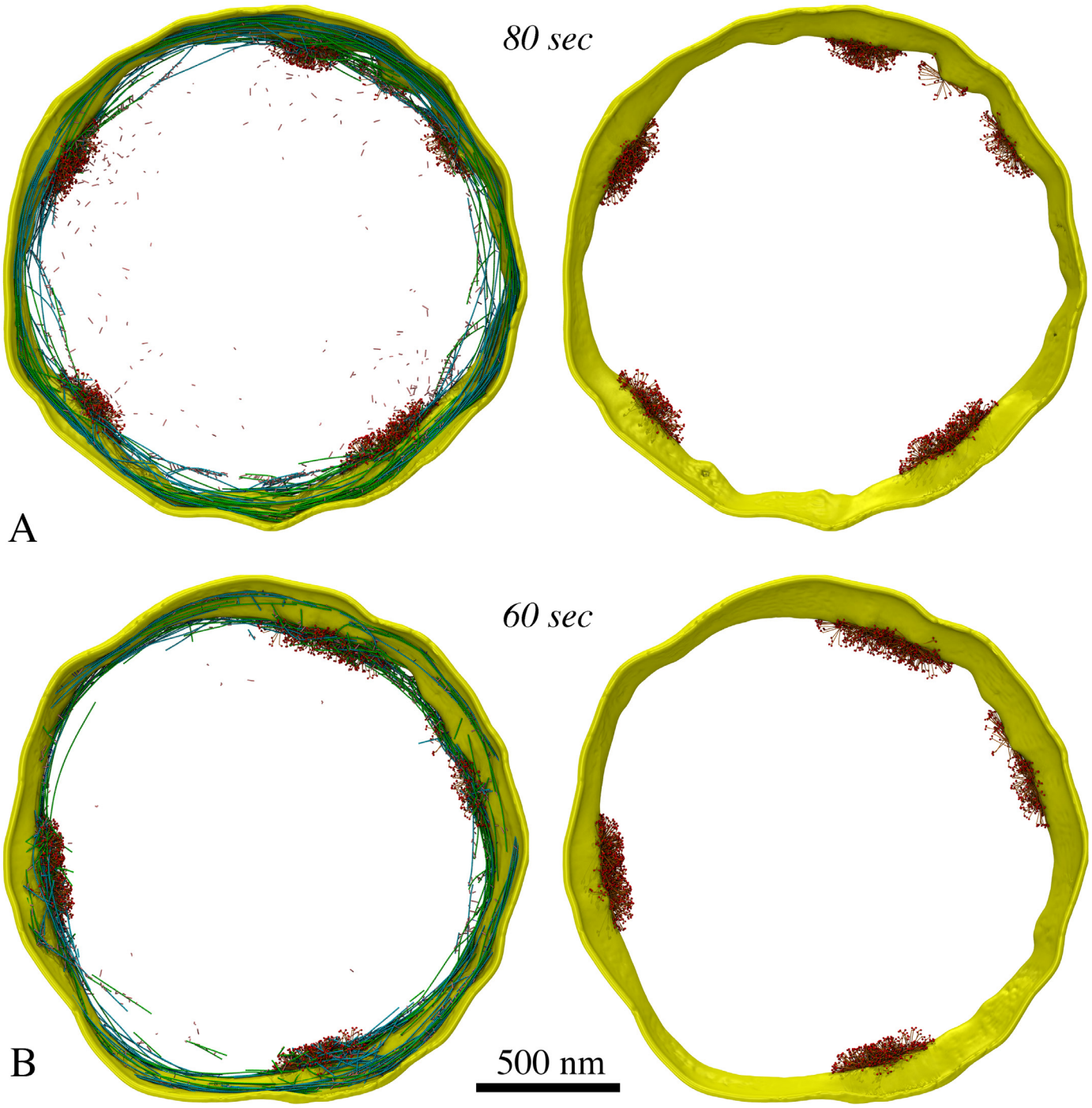

Figure S8: Enlarged views of simulation results of model 5 (A) and model 9 (B). The presence of nodes of unipolar myosin resulted in formation of large aggregates that distorted the membrane (right panels).

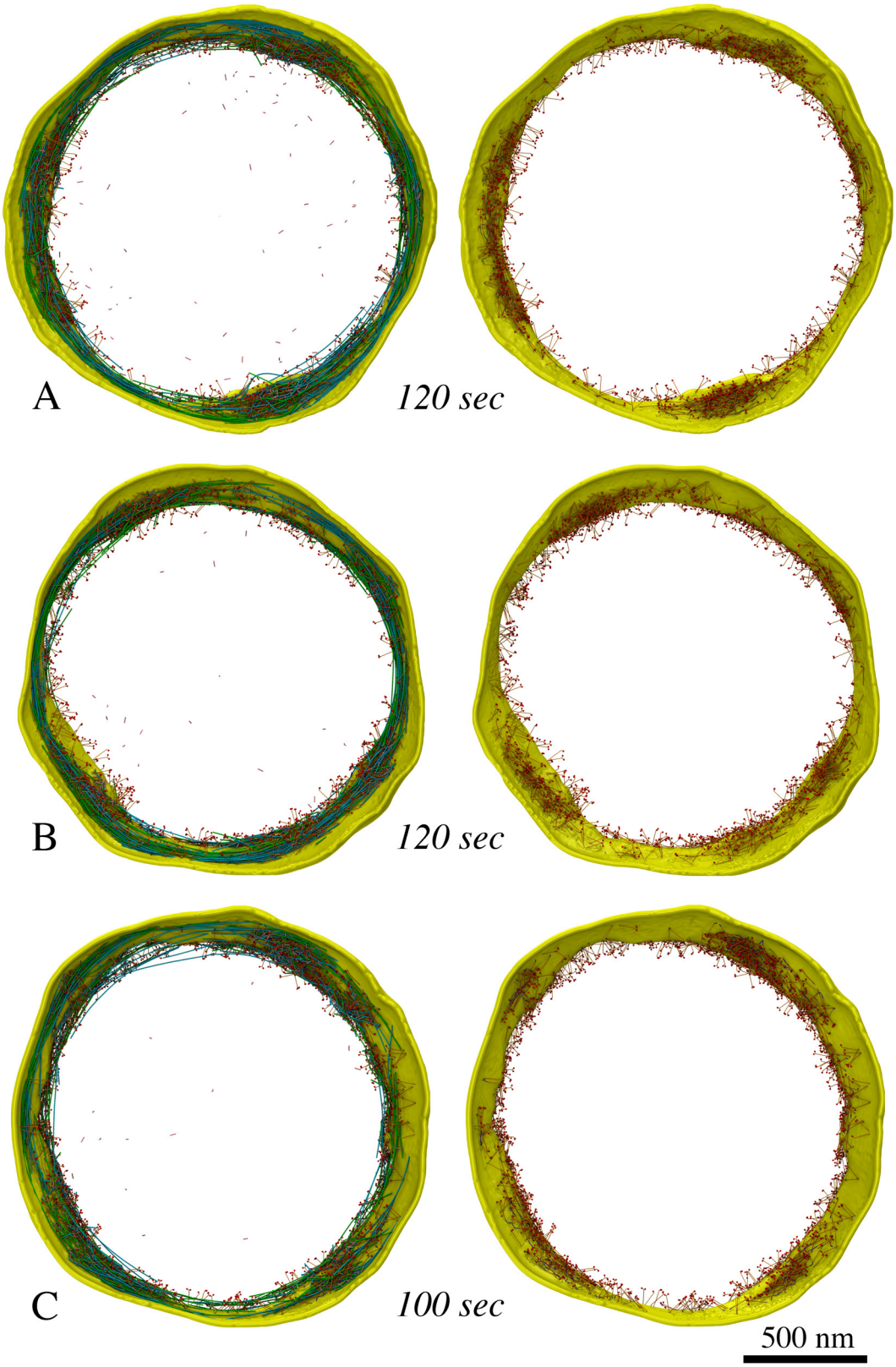

Figure S9: Enlarged views of simulation result of model 6 (A), model 10 (B), and model 14 (C). Unipolar myosin pairs aggregated into big clusters that distorted the membrane (right panels).

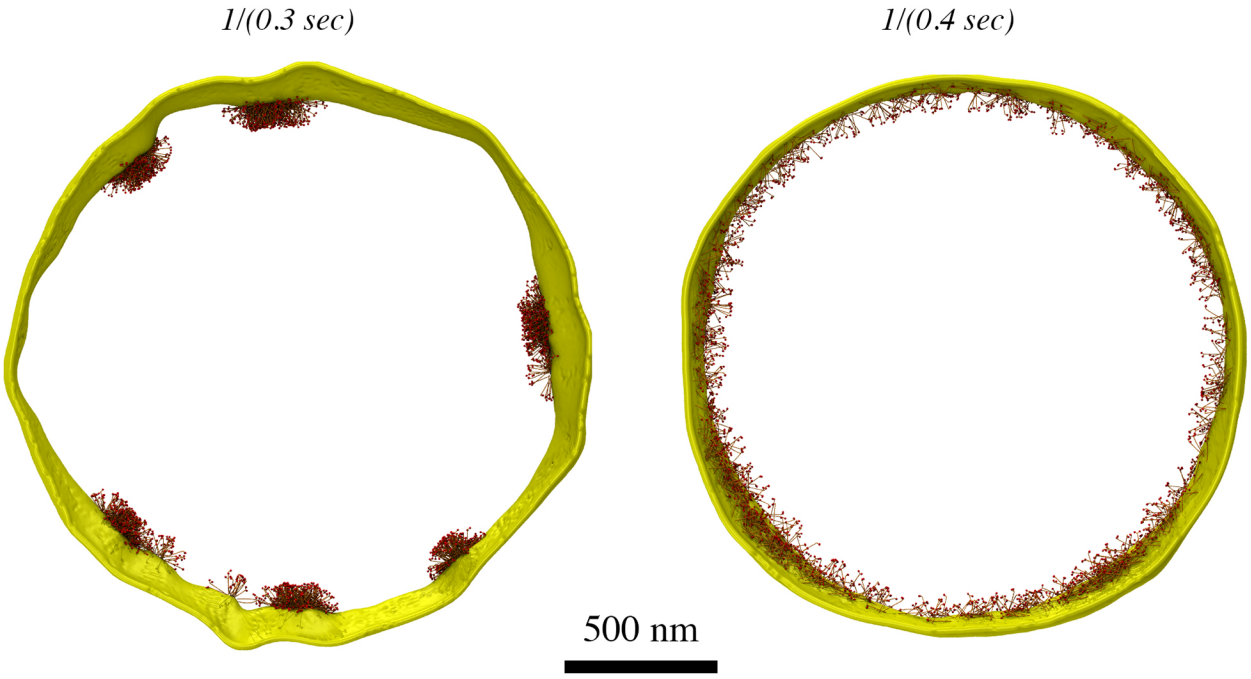

Figure S10: Simulation results at 60 sec of the simulated time at high myosin turnover rates (denoted by the numbers on the top of the panels). Even at a turnover rate > 40 times the experimental rate of 1/(14 sec) (see Fig. S11) myosin nodes (as in model 5) still aggregated (left). On the other hand, aggregation of myosin pairs (as in model 6) was mitigated at a turnover rate > 30 times the experimental rate (right).

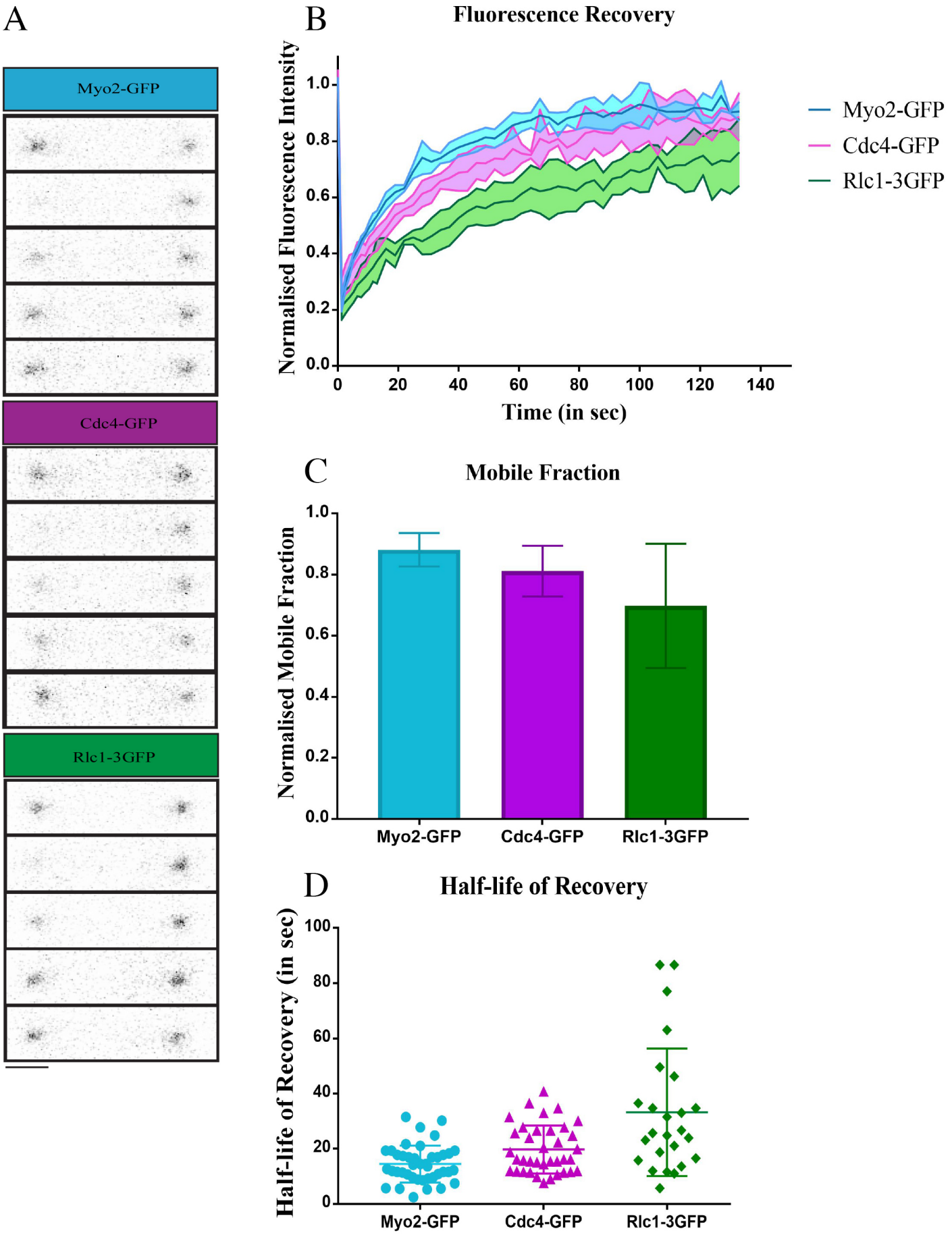
A
Myo2-GFP
Cdc4-GFP
Rlc1-3GFP
B
Fluorescence Recovery
Normalised Fluorescence Intensity
1.0
0.8
0.6
0.4
0.2
0.0
0
20
40
60
80
100
120
140
Time (in sec)
Myo2-GFP
Cdc4-GFP
Rlc1-3GFP
C
Mobile Fraction
Normalised Mobile Fraction
1.0
0.8
0.6
0.4
0.2
0.0
Myo2-GFP
Cdc4-GFP
Rlc1-3GFP
D
Half-life of Recovery
Half-life of Recovery (in sec)
100
80
60
40
20
0
Myo2-GFP
Cdc4-GFP
Rlc1-3GFP

74

Figure S11: Dynamic turnover of myosin components in the contractile ring. (A) Representative time-lapse images of fluorescence recovery after photobleaching in cells expressing Myo2-GFP (n=15), Cdc4-GFP (n=16) and Rlc1-GFP (n=14). (B) Quantification of fluorescence recovery with intensity normalized for photobleaching during acquisition. (C) Graphs representing the mobile fraction and (D) half-life of recovery, derived from single exponential fitting. All experiments were done in triplicates. Scale bar represents 2μm, and error bars indicate standard error of the mean. The experimental methods are described below.

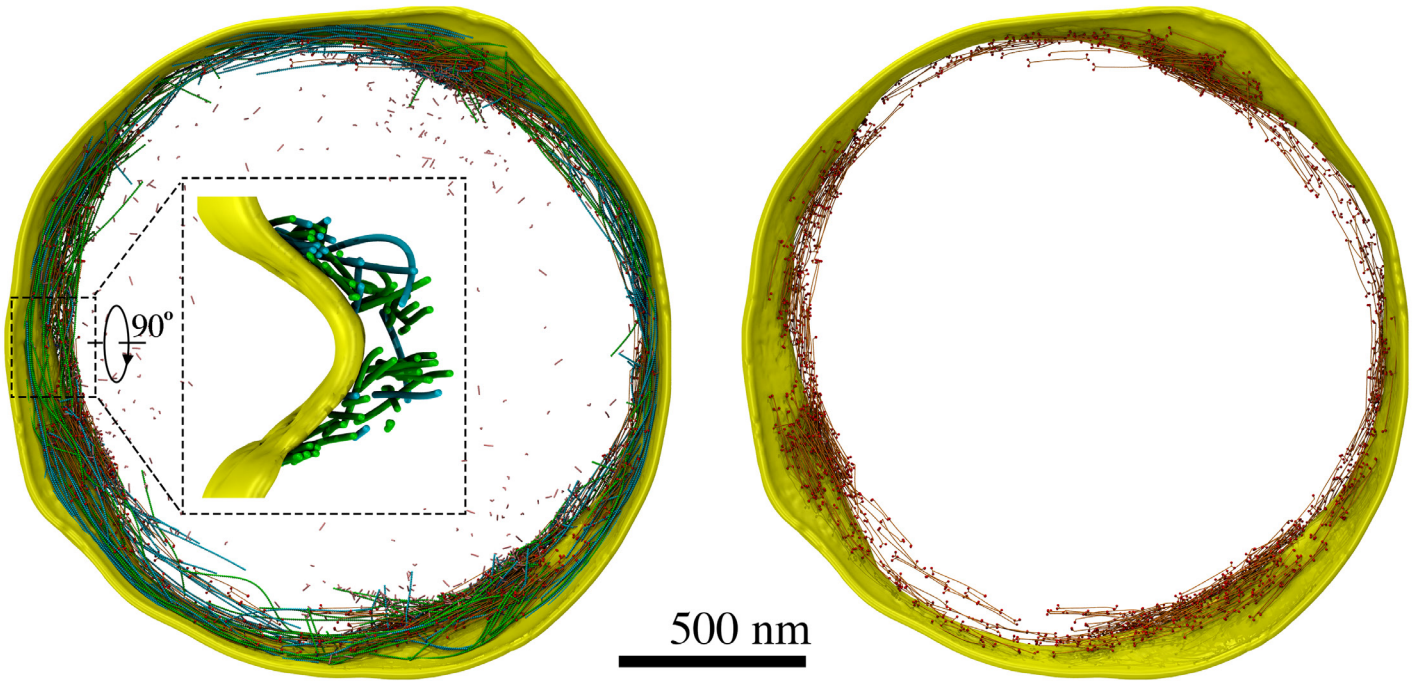

Figure S12: Enlarge views and additional views of simulation results of model 8 after 120 sec of the simulated time. (left) A zoomed-in view shows that some actin filaments were pulled away from the membrane. (right) Myosin aggregated in the locations of actin plus ends.

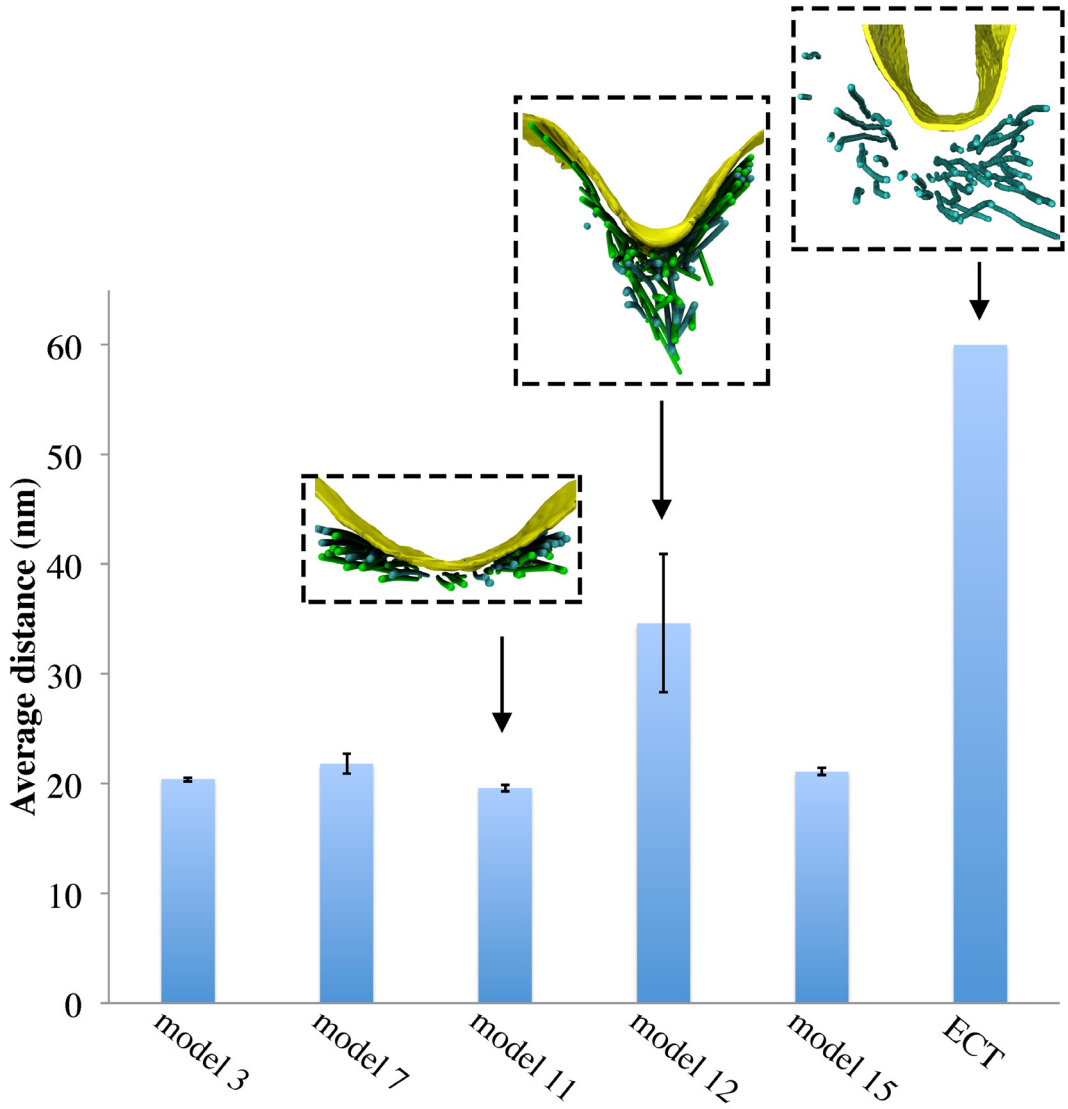

Figure S13: Actin-membrane distances, each averaged over five simulations with error bars representing standard deviation. While actin filaments were seen at an average distance of 60 nm from the membrane in tomograms, those in simulations were much closer. In the presence of membrane-attached unipolar myosin (models 3, 7, 11, and 15), all F-actin was within 60 nm, but the presence of bipolar myosin (model 12) pulled some F-actin (~ 10%) away from the membrane.

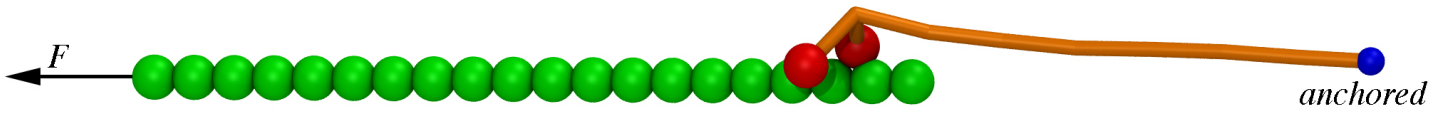

Figure S14: Simulation setup to determine myosin bending stiffness: a unipolar myosin walked on an actin filament of 20 beads starting from the minus end. In this setup the myosin tail was anchored and the actin plus end was pulled by a force F that was kept constant during each simulation. In the first set of simulations, F was set to be 3 pN if one myosin head was active while the other kept inert and 6 pN if both heads were active. Myosin's bending stiffness k_θ^m was then increased from $0.1 \cdot 10^{-18}$ J to $1.0 \cdot 10^{-18}$ J. Starting from $k_\theta^m = 0.5 \cdot 10^{-18}$ J, the myosin head could reach the actin plus end. In the second set of simulations k_θ^m was set to be $0.5 \cdot 10^{-18}$ J while F was varied from 1 pN to 10 pN. When a single myosin head was active, myosin stalled at $F \sim 3 - 4$ pN, similar to the value reported experimentally (Finer et al., 1994). When both myosin heads were active, myosin stalled at $F \sim 6 - 7$ pN. Based on these results, the bending stiffness was chosen to be $k_\theta^m = 0.5 \cdot 10^{-18}$ J. For each set of parameters tested, simulations of 5 sec each were repeated four times.

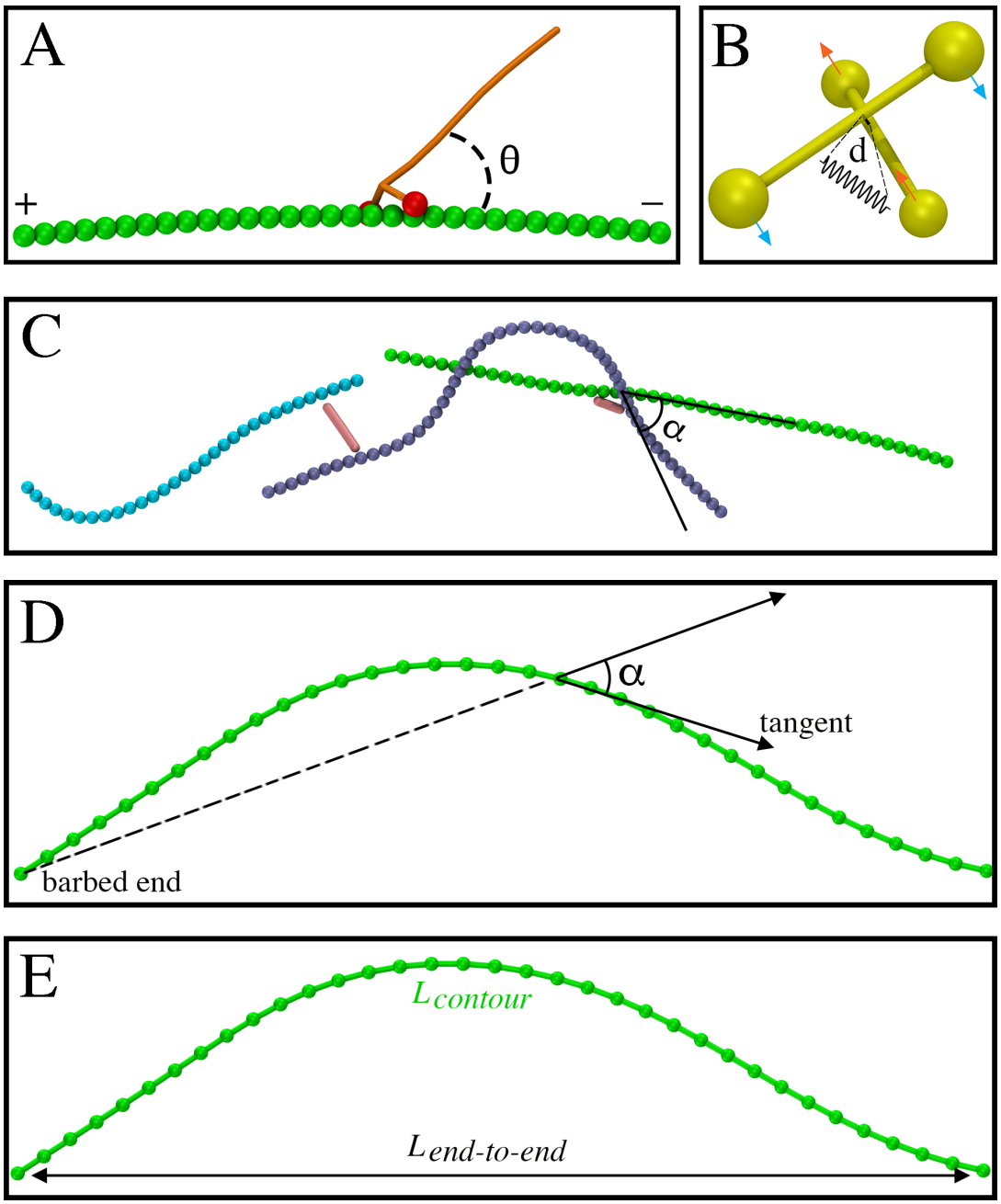

Figure S15: (A) Schematic of actomyosin interaction: in our simulations, myosin only binds to F-actin if θ is less than 90°. (B) Schematic of constraining four neighboring membrane beads to the same plane by two pairs of spring-like forces (arrows), one parallel and the other antiparallel to the distance vector ***d*** between the two diagonals. (C) The probability of crosslink release was a function of the angle α between the crosslinked filaments. (D) The probability of cofilin severing an F-actin was a function of the angle α between the tangent and the position vector from the barbed end. (E) The straightness of an actin filament was calculated as its end-to-end length divided by its contour length.

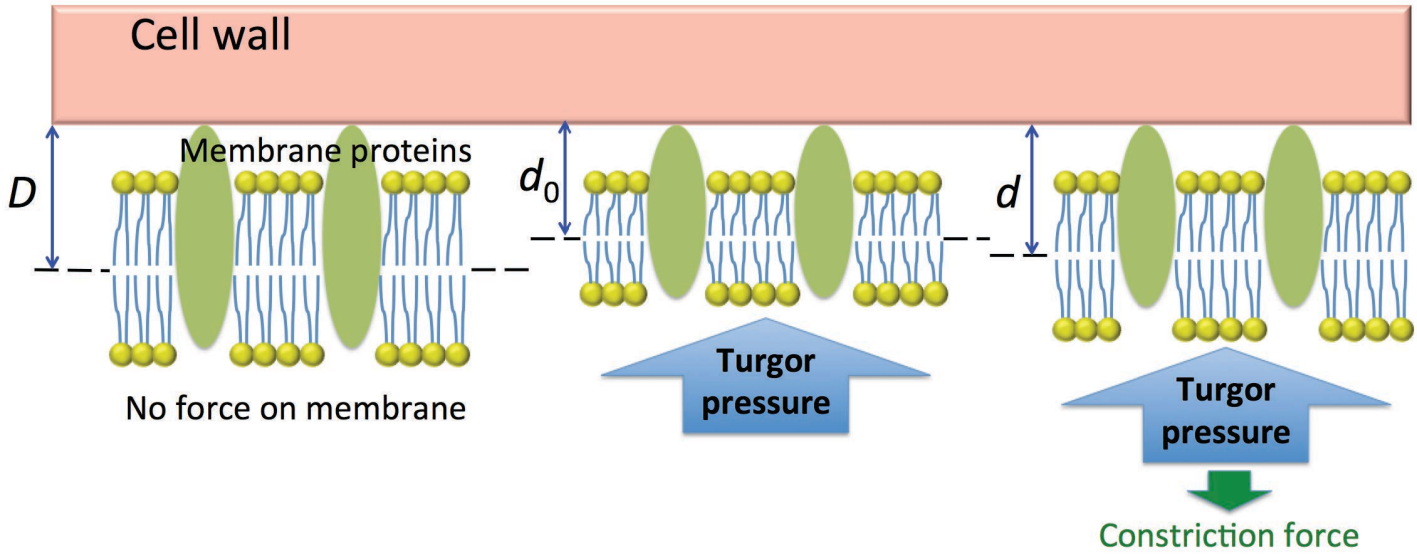

Figure S16: Schematic of our compressible model of the membrane. In the absence of force on the membrane, the distance between the membrane center and cell wall is D. Turgor pressure compresses the membrane and its associated proteins resulting in an equilibrium distance d_0. In our model, the constriction force from the actomyosin ring relaxes this distance slightly to d, stimulating inward growth of the cell wall. Note that for clarity, objects are not drawn to scale.

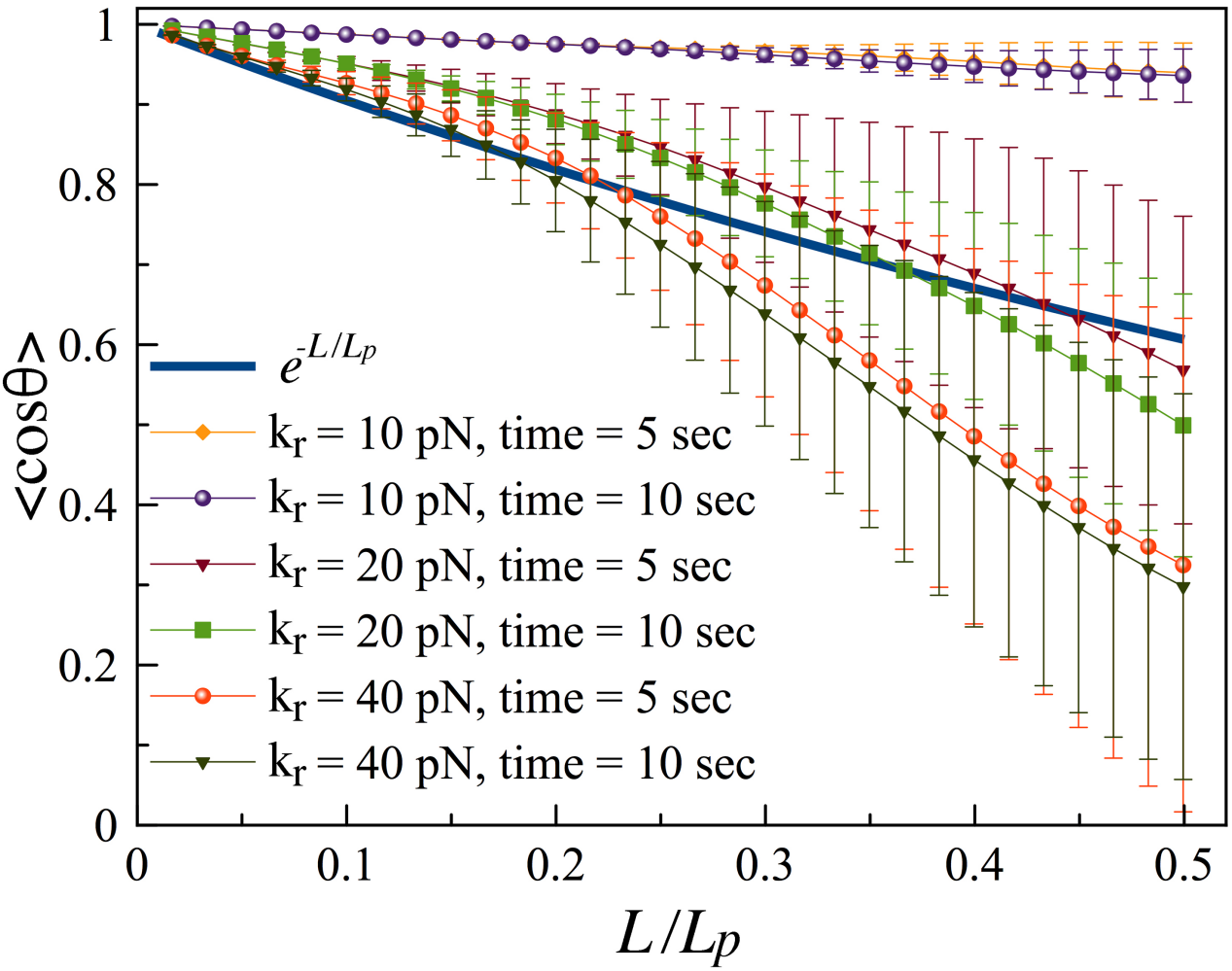

Figure S17: Tangent correlation $\langle cos\theta \rangle$ as a function of L/L_P where θ was the angle between the tangent vector at position 0 and the tangent vector at a distance L along the filament, L_P = 3.3 μm was the filament's persistence length (which was reduced three times from the original value and corresponding to the bending stiffness $k_\theta^a = 2.4 \cdot 10^{-18}$ J), and the theoretical tangent correlation function was e^{-L/L_P}. Simulations were run for 5 and 10 sec with different force constants k_r for the random force. The average was calculated over 4 simulations for each set of parameters. Error bars represent standard deviation.

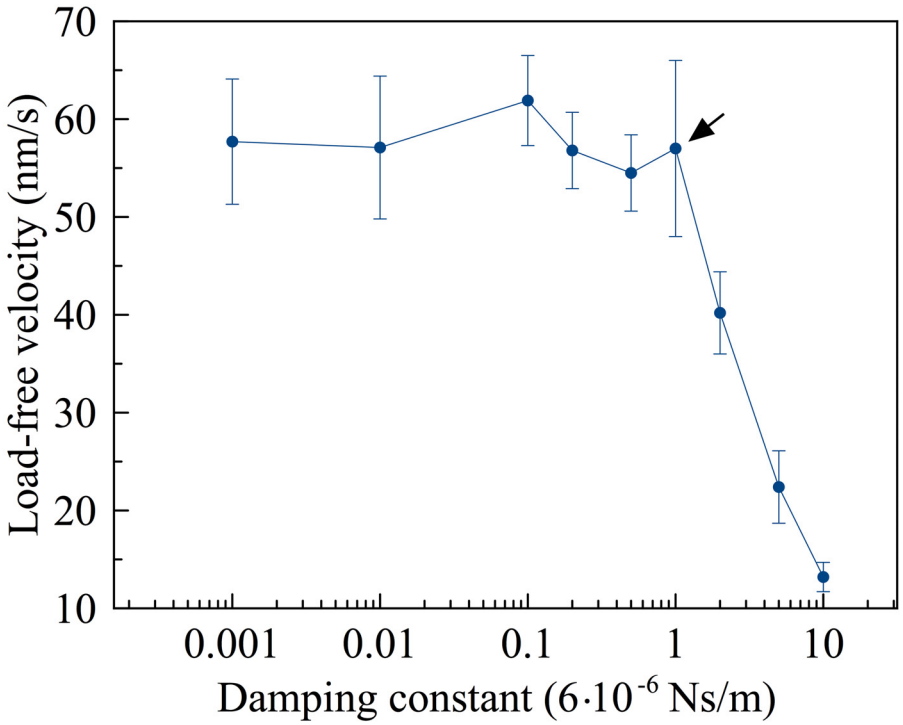

Figure S18: Dependence of the myosin load-free velocity on the damping constant. Arrow indicates the value chosen in our simulations. Note that in our model, as mentioned in **Methods/Myosin ATPase cycle**, the upper bound for the myosin load-free velocity was set by the ATPase rates to be ~ 70 nm/s.

Supplemental Table

Table S1: Myosin resident time *in silico* (turnover rate was defined as inverse of resident time). Simulations were run for each resident time of unbound myosins and then the average and standard error of the resultant total myosin's resident time (bound and unbound) on the ring were calculated. Calculations were done after 60 sec of the simulated time to allow several rounds of complete turnover. Values used in simulations that were used to produce figures are in **bolds**. Values in *italic*s correspond to myosin resident times that were significantly shorter than our experimentally-measured value of 14 s (Fig. S11), and * indicates values that mitigated aggregation.

	Resident time of unbound myosins (s)	Resultant resident time of all myosins (s) averaged over of 2 simulation runs. Values in *italics* were from single runs.
Model 1	2.8 **5.6**	8.95 ± 0.05 15.95 ± 0.55
Model 2	1.0 **1.4** 2.8	12.9 ± 0.9 16.8 ± 0.8 32.3 ± 1.9
Model 3	**7.0** 10.0	10.3 ± 0.2 15.25 ± 0.05
Model 4	0.2 **0.6**	12.3 ± 0.5 21.9 ± 1.7
Model 5	2.8 **5.6**	7.15 ± 0.05 14.4 ± 0.2
Model 6	1.0 **1.5** 2.0 *0.5* *0.2* *0.1**	8.9 ± 0.4 14.55 ± 0.05 19.0 ± 1.2 *3.9* *1.2* *0.4**
Model 7	2.8 **7.0**	5.45 ± 0.15 13.6 ± 0.4
Model 8	0.5 1.0 **1.5**	14.25 ± 0.05 22.6 ± 0.1 28.1 ± 0.5
Model 9	2.8 **5.6**	6.95 ± 0.05 12.8 ± 0.4
Model 10	**1.4** 2.8 *1.0* *0.5* *0.2**	9.0 ± 0.2 18.2 ± 1.5 *7.3* *3.2* *1.1**
Model 11	5.6 **8.0**	9.25 ± 0.05 13.2 ± 0.3

Model 12	**0.25** 0.5 1.0	8.65 ± 0.05 13.3 ± 0.2 23.7 ± 0.3
Model 13	2.8 **10.0**	5.75 ± 0.05 19.2 ± 0.9
Model 14	1.4 **2.8** *0.5* *0.2* *0.1**	9.2 ± 0.4 18.4 ± 0.3 *3.2* *1.0* *0.23**
Model 15	2.8 **7.0**	4.75 ± 0.05 12.9 ± 0.6
Final model	1.4 **5.6**	4.4 ± 0.2 15.7 ± 0.8

145

146 **Table S2:** Summary of key parameters used in simulations

147

Parameters	Justification
Actin spring's relaxed length (covering two actin monomers) $l_a = 5.5$ nm	Dominguez and Holmes, 2011
Actin spring constant $k_a = EA/l_a = 10$ nN/nm (estimating $A \sim 30$ nm^2)	$E = 1.8$ nN/nm^2 (Kojima et al., 1994)
Actin bending stiffness $k_\theta^a = k_B T L_p / l_a \sim 7.4 \cdot 10^{-18}$ J To reduce computational cost, a value of $2.4 \cdot 10^{-18}$ J was used in **Exploration of models**	$L_p \sim 10$ μm (Isambert et al., 1995)
Myosin spring's relaxed length $l_m = 10$ nm	Chosen to represent a segment of 10 nm
Myosin spring constant $k_m = 1$ nN/nm	Arbitrarily chosen to be 10 times smaller than k_a
Myosin bending stiffness $k_\theta^m = 0.5 \cdot 10^{-18}$ J	Arbitrarily chosen to be ~10 times smaller than k_θ^a
Myosin ATPase rates: ATP-bound to {ADP and hydrolyzed P_i}-bound: 25/s *(5/s and 2.5/s were also used to test myosin processivity)* {ADP, P_i}-bound to {ADP, P_i and actin}-bound: 50/s {ADP, P_i, actin}-bound to {ADP, actin}-bound: 25/s {ADP, actin}-bound to actin-bound: 25/s Actin-bound to ATP-bound: 150/s	De La Cruz and Ostap, 2009 Heissler et al., 2013
Crosslinkers modeled as two springs of length l_c and spring constant k_c: Fission yeast α-actinin length: $2l_c^\alpha = 22$ nm α-actinin spring constant: $k_c^\alpha = 0.5$ nN/nm Fimbrin length: $2l_c^f = 10$ nm Fimbrin spring constant $k_c^f = 1.1$ nN/nm	$2l_c^\alpha$ = 2 actin-binding domains (~5 nm each) plus 2 spectrin repeats (~6 nm each, PDB structure 4D1E). Note, human α-actinin has 4 spectrin repeats. k_c^α was chosen to be 20 times smaller than k_a $2l_c^f$ was estimated from PDB structure 1RT8 $k_c^f = k_c^\alpha \cdot l_c^\alpha / l_c^f$

Crosslinker's actin binding rate: 100/s	Arbitrarily chosen
α-actinin's actin unbinding rate: 3/s	A value in between 2.4/s (Xu et al., 1998) and 3.3/s (Li et al., 2016)
Fimbrin's actin unbinding rate: 0.05/s	Skau et al., 2011
Number of F-actins per ring cross-section: 30 – 40	To be within the 13 – 60 range shown by our electron cryotomography data (Swulius et al.).
Number of unipolar myosins: 1,600	In the range reported by Wu and Pollard, 2005
Number of bipolar myosins: 800	In the range reported by Wu and Pollard, 2005
Number of α-actinin: 300, 600*,1200	* In the range reported by Wu and Pollard, 2005
Number of fimbrins: 500, 1000*, 2000	* In the range reported by Wu and Pollard, 2005
Number of nodes: 64, 140	Vavylonis et al, 2008; Laplante et al., 2016
Actin depolymerization rate: 1 monomer/s	In the range reported by Pelham and Chang, 2002
Myosin turnover rate: once every 14 s	Our own measurement (Fig. S11)
Crosslinker turnover rate: once every 20 s	Laporte et al., 2012
Mechanosensitivity of cell wall growth: $F_m = 0.005 - 0.1$ pN	Tested in a large range

148

Supplemental References

Finer, J.T., Simmons, R.M., and Spudich, J.A. (1994). Single myosin molecule mechanics: piconewton forces and nanometre steps. Nature *368*, 113–119.